



Article

Evolutionary Computational Intelligence-Based Multi-Objective Sensor Management for Multi-Target Tracking

Shuang Liang ¹, Yun Zhu ^{2,*}, Hao Li ³ and Junkun Yan ⁴

¹ Academy of Advanced Interdisciplinary Research, Xidian University, Xi'an 710071, China; sliang@xidian.edu.cn

² School of Computer Science, Shaanxi Normal University, Xi'an 710119, China

³ School of Electronic Engineering, Xidian University, Xi'an 710071, China; haoli@xidian.edu.cn

⁴ National Laboratory of Radar Signal Processing, Xidian University, Xi'an 710071, China; jkyan@xidian.edu.cn

* Correspondence: yunzhu@snnu.edu.cn

Abstract: In multi-sensor systems (MSSs), sensor selection is a critical technique for obtaining high-quality sensing data. However, when the number of sensors to be selected is unknown in advance, sensor selection is essentially non-deterministic polynomial-hard (NP-hard), and finding the optimal solution is computationally unacceptable. To alleviate these issues, we propose a novel sensor selection approach based on evolutionary computational intelligence for tracking multiple targets in the MSSs. The sensor selection problem is formulated in a partially observed Markov decision process framework by modeling multi-target states as labeled multi-Bernoulli random finite sets. Two conflicting task-driven objectives are considered: minimization of the uncertainty in posterior cardinality estimates and minimization of the number of selected sensors. By modeling sensor selection as a multi-objective optimization problem, we develop a binary constrained evolutionary multi-objective algorithm based on non-dominating sorting and dynamically select a subset of sensors at each time step. Numerical studies are used to evaluate the performance of the proposed approach, where the MSS tracks multiple moving targets with nonlinear/linear dynamic models and nonlinear measurements. The results show that our method not only significantly reduces the number of selected sensors but also provides superior tracking accuracy compared to generic sensor selection methods.

Keywords: computational intelligence; intelligent sensing technique; multi-sensor systems; multi-target tracking; random finite set; sensor selection



Citation: Liang, S.; Zhu, Y.; Li, H.; Yan, J. Evolutionary Computational Intelligence-Based Multi-Objective Sensor Management for Multi-Target Tracking. *Remote Sens.* **2022**, *14*, 3624. <https://doi.org/10.3390/rs14153624>

Academic Editor: Danilo Orlando

Received: 6 July 2022

Accepted: 26 July 2022

Published: 28 July 2022

Publisher's Note: MDPI stays neutral with regard to jurisdictional claims in published maps and institutional affiliations.



Copyright: © 2022 by the authors. Licensee MDPI, Basel, Switzerland. This article is an open access article distributed under the terms and conditions of the Creative Commons Attribution (CC BY) license (<https://creativecommons.org/licenses/by/4.0/>).

1. Introduction

With the rapid development of sensing techniques, sensing systems with multi-sensor configurations have attracted lots of attention in numerous fields, such as scene analysis, military defense, habitat monitoring, and other surveillance scenarios [1–4]. As one of the most important techniques, multi-target tracking (MTT) in multi-sensor systems (MSSs) is challenging for two reasons. On the one hand, MTT itself is difficult due to target birth, target death, false alarm, miss detection, and data association uncertainty. On the other hand, due to communication and real-time constraints, intelligent sensor management is required to balance the constraints and the tracking accuracy. Under the complex, dynamic and variable circumstances, sensor control can be regarded as an optimal nonlinear control issue, and standard optimal control schemes are not directly applicable [5].

Conventional MTT approaches used in the literature can be regarded as combinations of single-target trackers. Examples of such approaches include multiple hypothesis tracking [6,7] and joint probabilistic data association [8]. However, they cannot be used in principled sensor management since it is difficult to formulate a management criterion that accommodates the multi-target in a mathematical description. A solution to solve the sensor management problem is to use finite set statistics (FISST) [9,10] in the Bayesian

paradigm. Under the framework of FISST, the multi-target probability density is used to describe the uncertainty of the multi-target system and can be systematically handled by random finite sets (RFSs). The probability hypothesis density (PHD) [11], cardinalized PHD [12], and multi-Bernoulli (MB) [13] filters are popular FISST-based approaches. The MB filter uses multiple independent Bernoulli RFSs to model the set of independent targets and propagates MB parameters over time. Different from the MB filter, the PHD and cardinalized PHD filters propagate moments of the multi-target posterior density. These filters were developed as crude approximations of the Bayes filter and cannot output the trajectory for each target. In [14,15], the labeled RFS was used to solve the problem of trajectory estimation. Following these studies, Vo et al. developed a multi-target tracker named generalized labeled MB (GLMB) [16]. The labeled MB (LMB) filter [17] proposed by Reuter et al. provides an efficient approximation of the GLMB filter. In terms of accuracy, the LMB filter outperforms the PHD, cardinalized PHD, and MB filters. What is more, it outputs target trajectories.

Several solutions have been proposed under the FISST framework to solve the sensor management problem. An objective function is generally required as a criterion for sensor management. The Rényi divergence [18–20], or alpha divergence, is widely used as the objective function for sensor management. The Kullback–Leibler divergence or Hellinger affinity are special cases of the Rényi divergence. Recently, a closed-form expression of the Cauchy–Schwartz divergence has been developed for Poisson densities [21], the GLMB filter [22], and the LMB filter [23], providing an alternative objective function for sensor management [22,24,25]. Although the information divergence is derived in a principled manner, it is unclear how to translate it directly into practical performance criteria such as state or cardinality estimation errors. To meet the task of sensor management in a direct way, the task-driven objective functions have been developed [23,26–29]. In [26], the cardinality variance was used to enable efficient sensor management. In [23], Gostar et al. proposed minimizing the posterior dispersion. To deal with multiple tasks simultaneously, ad hoc methods have been developed in [27–29] by estimating the relative importance of each task and assigning weights to the objective functions. It is necessary to estimate the relative importance of each task. In [30], Nguyen et al. studied the multi-objective path-planning problem and proposed competing objectives for searching for undiscovered moving targets while keeping track of discovered targets.

In this work, we consider the problem of selecting a subset of sensors acquiring high-quality measurements to alleviate the energy and bandwidth issues. For the sensor selection problem, it is usually assumed that the number of sensors to be selected is known in advance [31], as illustrated in Figure 1.

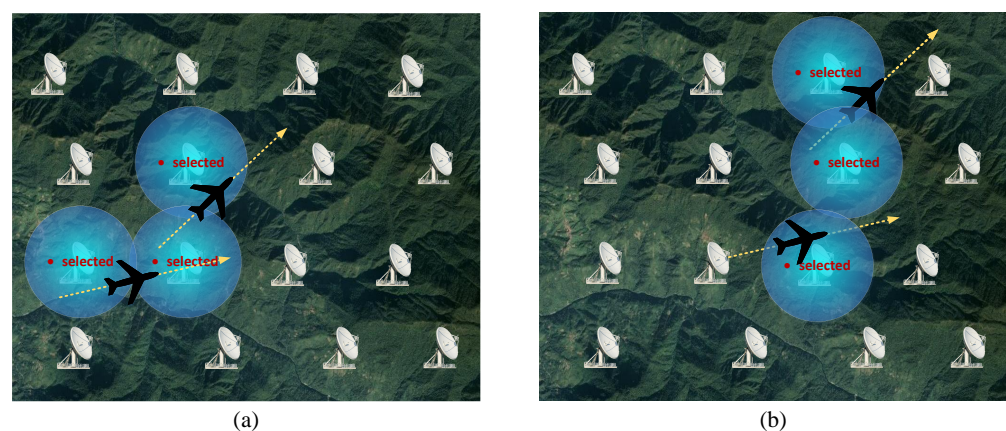


Figure 1. Illustration of dynamic selection of a fixed number of sensors for MTT: (a) At time k ; (b) At time $k + 1$. It is assumed that three sensors are selected at each time step, and the blue circles show the coverage areas of the selected sensors.

However, in most practical applications, such as multi-sensor MTT, it is impossible for the system's designer to know the exact number of selected sensors before the selection operation begins. Apparently, it is necessary to study a feasible sensor selection scheme that adaptively determines the optimal number of selected sensors according to the dynamics of a multi-sensor multi-target system. In this case, sensor selection is, in fact, a global combinatorial optimization problem. When the scale of the MSS is large, sensor selection can be extremely challenging. To alleviate this issue, a spatial non-maximum suppression algorithm has been proposed in [32], but its performance is affected by a tuning parameter. The work in [33] developed an approach that decoupled the multi-sensor coordinated management into distributed management of each sensor by maximizing the local Rényi divergence. This method can be used for distributed MTT but not for sensor selection. Wang et al. [34] proposed a guided search algorithm for multi-dimensional optimization-based sensor management. It is not applicable to sensor selection applications and may become stuck at a nonstationary point because of the use of coordinate descent. Cao et al. [35] proposed a sensor selection scheme with low computational complexity based on the upper bound of the mutual information. The method is only applicable for tracking a single target.

The aim of this study is to develop a methodology that allows selection of fewer sensors while ensuring the performance of MTT. The LMB filter is used for MTT by modeling the multi-target states as LMB RFSs. In the sensor selection procedure, we develop the number of selected sensors as an objective function. The variance of the cardinality distribution is also designed as an objective function to improve the accuracy of the cardinality estimate. In addition, a constraint of the number of selected sensors is necessary to meet communication constraints while guaranteeing the performance of the filter. However, minimizing the number of selected sensors and minimizing the cardinality variance is conflicting. The problem is further compounded by the number constraint. To solve this problem, we model it as a multi-objective optimization (MOO) problem and develop a binary constrained evolutionary multi-objective algorithm to dynamically select a subset of sensors. For each selection command, the generalized covariance intersection (GCI) scheme [36] is used for implementing multi-sensor data fusion. The main contributions are summarized as follows.

First, to the best of our knowledge, it is the first study in which an evolutionary algorithm is used in the multi-objective POMDP for MTT. In general, the ideal solution of the MOO does not exist since the objective functions are conflicting. We find the Pareto solutions using an evolutionary multi-objective algorithm via non-dominated sorting and dynamically select a subset of sensors at each time step.

Second, we develop a novel binary constrained crossover and binary constrained mutation operators within the evolutionary algorithm to handle the constraint for the number of selected sensors and obtain feasible solutions.

Third, we compare the proposed evolutionary MOO (EMOO)-based sensor selection approach with several other sensor selection solutions. Simulation results prove that the proposed approach has satisfactory state estimation performances and effectively reduces the number of selected sensors.

The paper is organized as follows. Section 2 presents the existing literature on the RFS and the LMB recursion. The motivation and implementation of the EMOO-based sensor selection approach are presented in Section 3. Section 4 presents numerical simulations and results. Conclusions are given in Section 5.

2. Background

2.1. Labeled RFS

In the stochastic multi-target system, the target state is modeled as an RFS. The single-target state and the multi-target state are denoted by x and X , respectively. It is difficult to output the trajectories of multiple targets only by using the representation of RFS, and we can only estimate the set of states at different time steps, i.e., $\{X_1, \dots, X_k\}$. To address this issue, the labeled RFS is introduced. In the labeled RFS, the target state is augmented

with a label ℓ . To distinguish between labeled and unlabeled entities, labeled entities are bold, e.g., \mathbf{x} and \mathbf{X} . At time k , the multi-target state \mathbf{X}_k consists of $N(k)$ single-target states $\mathbf{x}_{k,1}, \dots, \mathbf{x}_{k,N(k)}$ and the multi-target measurement Z_k consists of $M(k)$ measurements $z_{k,1}, \dots, z_{k,M(k)}$. Then, \mathbf{X}_k and Z_k are given as

$$\mathbf{X}_k = \{\mathbf{x}_{k,1}, \dots, \mathbf{x}_{k,N(k)}\} \in \mathcal{F}(\mathbb{X} \times \mathbb{L}), \tag{1}$$

$$Z_k = \{z_{k,1}, \dots, z_{k,M(k)}\} \in \mathcal{F}(\mathbb{Z}), \tag{2}$$

where $\mathcal{F}(\mathbb{Z})$ denotes the space of finite subsets of \mathbb{Z} , and \mathbb{X} , \mathbb{L} , and \mathbb{Z} denote the spaces for X , ℓ , and Z , respectively.

The multi-target posterior density $\pi_k(\mathbf{X}_k|Z_{1:k})$ is estimated by the Bayesian prediction and update [9,10]

$$\pi_{k|k-1}(\mathbf{X}_k|Z_{1:k-1}) = \int f_{k|k-1}(\mathbf{X}_k|\mathbf{X}) \pi_{k-1}(\mathbf{X}|Z_{1:k-1}) \delta \mathbf{X}, \tag{3}$$

$$\pi_k(\mathbf{X}_k|Z_{1:k}) = \frac{g_k(Z_k|\mathbf{X}_k) \pi_{k|k-1}(\mathbf{X}_k|Z_{1:k-1})}{\int g_k(Z_k|\mathbf{X}) \pi_{k|k-1}(\mathbf{X}|Z_{1:k-1}) \delta \mathbf{X}}, \tag{4}$$

where $Z_{1:k} = (Z_1, \dots, Z_k)$ represents the set of measurements accumulated to the current time; $\pi_{k|k-1}(\mathbf{X}_k|Z_{1:k-1})$ is the predicted density; $f_{k|k-1}(\cdot|\cdot)$ is the multi-target transition density, encapsulating multi-target motion, such as target birth/death and single-target motion; $g_k(\cdot|\cdot)$ is the multi-target likelihood, encapsulating system uncertainty, such as observation noise, data association uncertainty, and detection uncertainty. The integrals given in (3) and (4) are not ordinary integrals but set integrals. For a function $f : \mathcal{F}(\mathbb{X} \times \mathbb{L}) \rightarrow \mathbb{R}$, the set integral is denoted as [9,10]

$$\int \mathbf{f}(\mathbf{X}) \delta \mathbf{X} = \sum_{i=0}^{\infty} \frac{1}{i!} \int \mathbf{f}(\{\mathbf{x}_1, \dots, \mathbf{x}_i\}) d(\mathbf{x}_1, \dots, \mathbf{x}_i). \tag{5}$$

In the following, the standard inner product notation of f and g is expressed as

$$\langle f, g \rangle \triangleq \int f(x)g(x)dx, \tag{6}$$

and the multi-target exponential notation is given as

$$h^{\mathbf{X}} \triangleq \prod_{x \in \mathbf{X}} h(x). \tag{7}$$

The inclusion function $1_S(X)$ and the Kronecker delta function $\delta_S(X)$ are denoted as

$$1_S(X) \triangleq \begin{cases} 1, & \text{if } X \subseteq S \\ 0, & \text{otherwise} \end{cases}, \quad \delta_S(X) \triangleq \begin{cases} 1, & \text{if } X = S \\ 0, & \text{otherwise} \end{cases}. \tag{8}$$

2.2. Labeled Multi-Bernoulli Filter

In the LMB filter, a target $x \in \mathbb{X}$ with label $\ell \in \mathbb{L}$ is completely characterized by the probability of existence $r^{(\ell)}$ and the probability density $p^{(\ell)}(x)$. The LMB distribution is, therefore, represented by $\pi = \{(r^{(\ell)}, p^{(\ell)}(\cdot))\}_{\ell \in \mathbb{L}}$. Let $\Delta(\mathbf{X}) = \delta_{|\mathbb{X}|}(|\mathcal{L}(\mathbf{x})|)$ denote a distinct label indicator and $\mathcal{L} : \mathbb{X} \times \mathbb{L} \rightarrow \mathbb{L}$ be the projection $\mathcal{L}(\mathbf{X}) = \{\mathcal{L}(x) : (x \in \mathbf{X})\}$. The LMB RFS density is parameterized as

$$\pi(\mathbf{X}) = \Delta(\mathbf{X})w(\mathcal{L}(\mathbf{X})) [p]^{\mathbf{X}}, \tag{9}$$

where

$$w(L) = \prod_{i \in \mathbb{L}} (1 - r^{(i)}) \prod_{i \in L} \frac{1_{\mathbb{L}} r^{(i)}}{(1 - r^{(i)})}, \tag{10}$$

$$[p]^X = \prod_{(x,\ell) \in X} p^{(\ell)}(x), \tag{11}$$

and L indicates a set of labels.

If the posterior density follows the LMB distribution and is parameterized as $\pi = \{ (r^{(\ell)}, p^{(\ell)}(\cdot)) \}_{\ell \in \mathbb{L}}$ and the birth model also follows the LMB distribution with the parameter set $\pi_B = \{ (r_B^{(\ell)}, p_B^{(\ell)}(\cdot)) \}_{\ell \in \mathbb{B}}$, then the predicted density is given as

$$\pi_+ = \{ (r_{+,s}^{(\ell)}, p_{+,s}^{(\ell)}(\cdot)) \}_{\ell \in \mathbb{L}} \cup \{ (r_B^{(\ell)}, p_B^{(\ell)}(\cdot)) \}_{\ell \in \mathbb{B}}, \tag{12}$$

where

$$r_{+,s}^{(\ell)} = \eta_S(\ell) r^{(\ell)}, \tag{13}$$

$$p_{+,s}^{(\ell)}(\cdot) = \frac{\langle p_S(\cdot, \ell) f(x|\cdot, \ell), p(\cdot, \ell) \rangle}{\eta_S(\ell)}, \tag{14}$$

$$\eta_S(\ell) = \langle p_S(\cdot, \ell), p(\cdot, \ell) \rangle, \tag{15}$$

$p_S(\cdot, \ell)$ is the state-dependent survival probability and $f(x|x', \ell)$ denotes the transition density of the target with track ℓ . For simplicity, we denote the predicted LMB RFS by

$$\pi_+ = \{ (r_+^{(\ell)}, p_+^{(\ell)}(\cdot)) \}_{\ell \in \mathbb{L}_+}, \tag{16}$$

where the label space $\mathbb{L}_+ = \mathbb{L} \cup \mathbb{B}$ (with $\mathbb{L} \cap \mathbb{B} = \emptyset$).

The family of the LMB RFS is closed under the Bayesian prediction but not closed under the Bayesian update. To solve this problem, the predicted LMB distribution is converted to a δ -GLMB distribution. Then, the update of the δ -GLMB is implemented, and the result is approximated by an LMB. The LMB approximation of the multi-target posterior density is denoted as

$$\pi(\cdot|Z) = \{ (r^{(\ell)}, p^{(\ell)}(\cdot)) \}_{\ell \in \mathbb{L}_+}, \tag{17}$$

where

$$r^{(\ell)} = \sum_{(I_+, \theta) \in \mathcal{F}(\mathbb{L}_+) \times \Theta_{I_+}} w^{(I_+, \theta)}(Z) 1_{I_+}(\ell), \tag{18}$$

$$p^{(\ell)}(x) = \frac{1}{r^{(\ell)}} \sum_{(I_+, \theta) \in \mathcal{F}(\mathbb{L}_+) \times \Theta_{I_+}} w^{(I_+, \theta)}(Z) \times 1_{I_+}(\ell) p^{(\theta)}(x, \ell), \tag{19}$$

$$w^{(I_+, \theta)}(Z) \propto w_+(I_+) [\eta_Z^{(\theta)}(\ell)]^{I_+}, \tag{20}$$

$$p^{(\theta)}(x, \ell|Z) = \frac{p_+(x, \ell) \psi_Z(x, \ell; \theta)}{\eta_Z^{(\theta)}(\ell)}, \tag{21}$$

$$\eta_Z^{(\theta)}(\ell) = \langle p_+(\cdot, \ell), \psi_Z(\cdot, \ell; \theta) \rangle, \tag{22}$$

$$\psi_Z(x, \ell; \theta) = \begin{cases} \frac{p_D(x, \ell) g(z_{\theta(\ell)}|x; \ell)}{\kappa(z_{\theta(\ell)})}, & \text{if } \theta(\ell) > 0, \\ 1 - p_D(x, \ell), & \text{if } \theta(\ell) = 0, \end{cases} \tag{23}$$

and Θ_{I_+} is the space of mappings $\theta : I_+ \rightarrow \{0, 1, \dots, |Z|\}$, such that $\theta(i) = \theta(i') > 0$ implies $i = i'$; $\kappa(\cdot)$ is the intensity of the clutter measurements; $g(z|x; \ell)$ is the likelihood of measurement z given (x, ℓ) .

In the sequential Monte Carlo (SMC) implementation, the density for each target with label (ℓ) is approximated by a weighted sum of particles, as follows

$$p^{(\ell)}(x) \simeq \sum_{j=1}^{J^{(\ell)}} \omega_j^{(\ell)} \delta_{x_j^{(\ell)}}(x), \tag{24}$$

where $\omega_j^{(\ell)}$ is the weight of particle j , and $J^{(\ell)}$ denotes the number of particles. For more details on the SMC implementation, please refer to [17].

3. Method

3.1. Objective Functions Proposal

Using sensor networks with communication constraints, sensor selection for MTT applications is usually employed to acquire the best set of measurements. As sensor management solutions, the Markov decision process and partially observable Markov decision process (POMDP) have received great attention over the last few decades [24]. The POMDP framework enables direct generalization to multiple targets by using the RFS model [9,10,24]. We model the sensor selection problem as the following discrete-time POMDP:

$$\Psi = \{\mathbf{X}_k, \mathbb{S}, f_{k|k-1}(\mathbf{X}_k|\mathbf{X}_{k-1}), g_k(Z_k|\mathbf{X}_k), \vartheta(s_k)\}, \quad (25)$$

where \mathbb{S} denotes a finite set of candidate sensors and $\vartheta(s_k)$ is the objective (reward or cost) function. In stochastic filtering, the aim is to find a selection command that optimizes $\vartheta(s_k)$.

In our work, two objective functions are considered: the number of selected sensors and the variance of the cardinality distribution. Both of the objective functions are dependent on binary decision variables. Let

$$s_k = [s_{1,k}, s_{2,k}, \dots, s_{N_s,k}], \quad (26)$$

be the selection command at time k , and N_s is the number of all candidate sensors in the MSS. The elements of s_k are binary variables, i.e., $s_{i,k} = 1$, if sensor s_i is selected and $s_{i,k} = 0$ otherwise. For example, if there are ten sensors in the system, $s_k = [0, 1, 0, 1, 0, 0, 0, 0, 1, 0]$ indicates the command that the sensors s_2 , s_4 and s_9 are selected at time k .

In many practical applications, the number of sensors to be selected is unknown to the system designer. To control the number of selected sensors at time k , the following objective function is considered

$$f_1(s_k) = \sum_{i=1}^{N_s} s_{i,k}. \quad (27)$$

The other objective function is the variance of the cardinality distribution, aiming at minimizing the error for the estimated number of targets. At time k , the cardinality variance corresponding to the selection command s_k is given by

$$f_2(s_k) = \sum_{\ell \in \mathbb{L}_+} r^{(\ell)}(s_k)[1 - r^{(\ell)}(s_k)]. \quad (28)$$

The objective function defined in (28) is computed using parameters of the updated LMB distribution. However, sensors have not been selected and it is impossible to update the LMB RFS density using measurements collected by the selected sensors. The predicted ideal measurement set (PIMS) strategy [37] is utilized to address this issue, which is dependent on the predicted LMB distribution and ideal assumption of perfect detection, no clutter, and no measurement noise. First, the predicted LMB distribution is used to estimate the number of targets and the target states. The maximum a posteriori estimate of the target number is computed as follows,

$$\hat{n} = \arg \max_n \rho(n) = \arg \max_n \rho(0) \sum_{L \subseteq \mathbb{L}, |L|=n} \left(\prod_{\ell \in L} \frac{r_+^{(\ell)}}{1 - r_+^{(\ell)}} \right), \quad (29)$$

where $\rho(0) = \prod_{\ell \in \mathbb{L}} (1 - r_+^{(\ell)})$. Then, we obtain \hat{n} labels with the highest existence probabilities from the predicted LMB distribution. The a posteriori estimate of the target state with label ℓ is given as

$$\hat{x}^{(\ell)} = \sum_{j=1}^{J_+^{(\ell)}} \omega_{j_+}^{(\ell)} x_{j_+}^{(\ell)}. \quad (30)$$

A predicted ideal measurement is estimated for each $\hat{x}^{(\ell)}$ under the assumed ideal conditions, and the pseudo-update of the LMB distribution is implemented with the PIMS. Then, the objective function (28) is computed using the generated pseudo LMB distribution.

3.2. Evolutionary Multi-Objective Optimization

Although the number of sensors to be selected is kept unknown, the number of selected sensors should be limited to a range N_{\min} and N_{\max} . This limit not only guarantees the performance of the filter but also meets the communication requirement. At time k , the constrained MOO is mathematically described as follows

$$\text{Minimize } F(s_k) = [f_1(s_k), f_2(s_k)]^T \quad (31)$$

$$\text{Subject to } N_{\min} \leq f_1(s_k) \leq N_{\max} \quad (32)$$

where $F(s_k)$ is the objective vector.

For the MOO problem, the solutions satisfying the constraint of (32) form the feasible set. The ideal solution is the one that is optimal for all the objective functions. In general, the ideal solution does not exist since the objective functions are conflicting. Several methods have been proposed to handle the problem [38–41]. Among them, the scalarization and Pareto methods do not need complicated numerical derivations and are widely used. The scalarization method is easy to implement, but it needs to assign relative weight to each objective based on prior information. Worse, unless the search space is convex, the solution may not be found [42]. In the Pareto method, the goodness of a solution is determined by the dominance, and a compromise solution can be found along the Pareto optimal front. We solve the above MOO problem and find optimal Pareto solutions using an evolutionary multi-objective algorithm via non-dominated sorting. First, the initial population of size N^{pop} is generated in which each solution is a feasible solution, represented by a vector of N_s binary elements. Then, the offspring solutions are obtained by binary tournament selection, crossover and mutation operators.

In our problem with binary decision variables, a simple crossover operator called one-point crossover is used. Two parent chromosomes and a random/given point are selected. After the given/selected point, genes of parent chromosomes are interchanged. An example is given in Figure 2, in which point four is selected, and the genes of two-parent chromosomes P1 and P2 are interchanged. Assuming that the number of selected sensors is limited to the range $N_{\min} = 1$ and $N_{\max} = 3$, we can observe that the offspring solutions in Figure 2 meet the constraints of the number of selected sensors. However, there are some cases where the offspring solutions need to be modified. An example is given in Figure 3, where the parent chromosomes P1 and P2 are different from those in Figure 2. In Figure 3, we also select point four and interchange the genes of P1 and P2. The sum of all the bits in solutions C1 and C2 are $N = 0$ and $N = 4$, respectively. Apparently, these solutions cannot meet the constraints of $N_{\min} = 1$ and $N_{\max} = 3$ and, hence, are infeasible for sensor selection. To solve this problem, we develop a binary constrained crossover procedure, as shown in Algorithm 1.

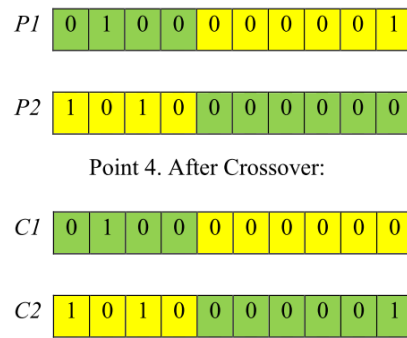


Figure 2. Example of the effective one-point crossover.

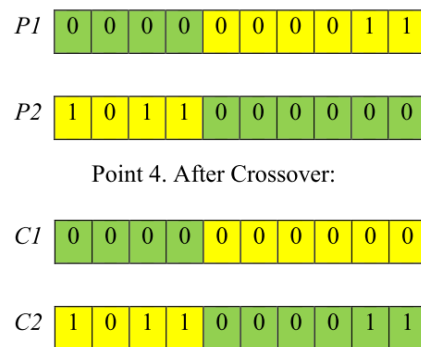


Figure 3. Example of the ineffective one-point crossover.

Algorithm 1 Binary constrained crossover.

1. Select one crossover point.
 2. Copy the binary string from the beginning to the crossover point of the first parent and the rest from the other parent.
 3. Compute the sum N of all the bits of the child solution.
 4. If $N_{\min} \leq N \leq N_{\max}$, the child solution is reserved; otherwise, go to line 5.
 5. Select and flip a point of the child solution, and go back to line 3.
-

Along with the binary constrained crossover, the mutation is also performed. For the binary issue, the bit flip mutation is one of the most commonly used mutation operators. In the bit flip mutation, one or more random bits are selected and then flipped. Figure 4 illustrates an example in which point four is selected from the parent chromosome P and flipped. We assume that the number of selected sensors is limited to the range $N_{\min} = 1$ and $N_{\max} = 3$. Then, the offspring solution in Figure 4 meets the constraints. There are some cases where the offspring solutions of the mutation need to be modified. Figure 5 shows an example, where we also select point four and flip it. The sum of all the bits in solution C is $N = 4$, which cannot meet the constraint of $N_{\max} = 3$. To solve this problem, we develop the binary constrained mutation, as shown in Algorithm 2.

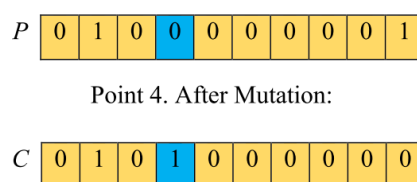


Figure 4. Example of the effective bit flip mutation.

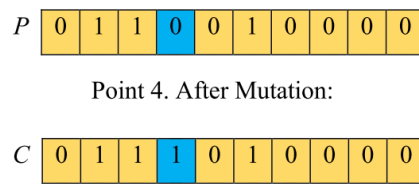


Figure 5. Example of the ineffective bit flip mutation.

Algorithm 2 Binary constrained mutation.

1. Randomly select one mutation point.
 2. Flip the selected mutation point.
 3. Compute the sum N of all the bits of the child solution.
 4. If $N_{\min} \leq N \leq N_{\max}$, the child solution is reserved; otherwise, go back to line 1.
-

After the variants (crossover and mutation), the offspring for the next generation are generated. The new population formed by the parents and offspring is sorted according to the non-dominant relationships. The size of the population is decreased to N^{pop} by eliminating the solutions with lower ranks. For the next generation, the new population is generated using binary tournament selection, binary constrained crossover, and binary constrained mutation. After several generations G , the Pareto-front is obtained.

The Pareto front is formed from non-dominated solutions, and it is necessary to choose one compromise solution from them. We use the gray relational analysis (GRA) strategy [43] to find the compromise solution. GRA does not require the weight of each objective function or other prior information. The gray relational coefficient (GRC) approach is used to estimate the similarity between the candidate network (formed by values of the objective functions for the Pareto solutions) and the optimal reference network (formed by the optimal value of each objective). Assuming that there are m Pareto solutions obtained by the evolutionary algorithm, f_{ij} is the i th value of the j th objective in the objective matrix, \bar{f}_{ij} is the value of f_{ij} after normalization. The main steps involved in GRA are summarized as follows.

i: Normalizethe objective function values of Pareto solutions, as follows

$$\bar{f}_{ij} = \frac{\max_{i \in m} f_{ij} - f_{ij}}{\max_{i \in m} f_{ij} - \min_{i \in m} f_{ij}}. \tag{33}$$

ii: Find the reference network points

$$f_j^* = \max_{i \in m} \bar{f}_{ij}. \tag{34}$$

iii: Estimate the difference between f_j^* and \bar{f}_{ij}

$$\Delta I_{ij} = |f_j^* - \bar{f}_{ij}|. \tag{35}$$

iv: Find the value of GRC for each optimal solution:

$$GRC_i = \frac{1}{m} \sum_{j=1}^n \frac{\Delta \min + \Delta \max}{\Delta I_{ij} + \Delta \max}, \tag{36}$$

where $\Delta \max = \max_{i \in m, j \in n} (\Delta I_{ij})$ and $\Delta \min = \min_{i \in m, j \in n} (\Delta I_{ij})$. v: Find the largest GRC_i , and the corresponding solution is recommended.

3.3. Multi-Sensor Fusion

For each selection command candidate $s \subseteq \mathbb{S}$, the posteriors are LMB RFSs with parameters $\pi(\cdot | Z^{(s)}) = \{ \{ \{ r_{i,s_i}^{(\ell)}, p_{i,s_i}^{(\ell)}(\cdot) \}_{\ell \in \mathbb{L}_+} \}_{i=1}^{|s|} \}$. The posterior density of each selected sensor is approximated by

$$p_{i,s_i}^{(\ell)}(x) = \sum_{j=1}^{J_+^{(\ell)}} \omega_{i,s_i,j}^{(\ell)} \delta_{x_{j_+}^{(\ell)}}(x). \quad (37)$$

During the update step of the LMB filter, the weights of particles are updated but the particles themselves are not changed. Therefore, the particles in (37) are the same particles used in the prediction.

We use the GCI scheme [36] to fuse those posterior LMB densities, which returns the following existence probabilities and densities,

$$r_s^{(\ell)} = \frac{\int \prod_{i=1}^{|s|} (r_{i,s_i}^{(\ell)} p_{i,s_i}^{(\ell)}(x))^{\omega_i} dx}{\prod_{i=1}^{|s|} (1 - r_{i,s_i}^{(\ell)})^{\omega_i} + \int \prod_{i=1}^{|s|} (r_{i,s_i}^{(\ell)} p_{i,s_i}^{(\ell)}(x))^{\omega_i} dx}, \quad (38)$$

$$p_s^{(\ell)}(x) = \frac{\prod_{i=1}^{|s|} (p_{i,s_i}^{(\ell)}(x))^{\omega_i}}{\int \prod_{i=1}^{|s|} (p_{i,s_i}^{(\ell)}(x))^{\omega_i} dx}, \quad (39)$$

where ω_i is a weight indicating the importance of sensor s_i in the fusion process. The sum of all the weights is equal to 1, i.e., $\sum_{i=1}^{|s|} \omega_i = 1$. We assume that all the sensors have equal importance in the simulation studies, i.e., $\omega_i = 1/|s|$. When using the particle approximation (37) to represent each LMB density, the integrals in (38) and (39) turn to weighted sums over the particles.

3.4. Step-by-Step Implementation

We introduce a sensor selection solution for MTT in this paper. The framework consists of four main steps: prediction, estimation of PIMS, EMOO-based sensor selection, and fusion of local posteriors. The schematic diagram is shown in Figure 6.

Algorithm 3 shows a complete step-by-step pseudocode for a single run of the proposed algorithm that outputs a fused LMB posterior. Assume that the following parameters are always available:

- Sensor model parameters: the number of candidate sensors N_s and their positions $s^{(j)} = [s_x, s_y]^T$, detection probabilities $p_D^{(j)}(\cdot)$, and clutter intensities $\kappa^{(j)}(\cdot)$ with $j = 1, 2, \dots, N_s$;
- Birth model parameters: $\{r_B^{(\ell)}, \{\omega_{j,B}^{(\ell)}, x_{j,B}^{(\ell)}\}_{j=1}^{J_B^{(\ell)}}\}_{\ell \in \mathbb{B}}$;
- Likelihood $g(z|x, \ell)$ and transition density $f(x|\cdot, \ell)$;
- Survival probability function: $p_S(x, \ell)$;
- Constraints on the number of selected sensors: N_{\min} and N_{\max} .

Similar to the standard particle filter, particle degeneracy is inevitable [44]. To alleviate the particle degradation problem, the particles for each hypothesized track are resampled in line 12. In a typical particle filtering implementation, Markov chain Monte Carlo steps are performed after resampling to improve the diversity of particles [44]. In line 13, multi-target states are extracted from the posterior LMB distribution and are used for error performance evaluation. The pseudocode of the algorithm for the EMOO-based sensor selection in line 6 is given in Algorithm 4.

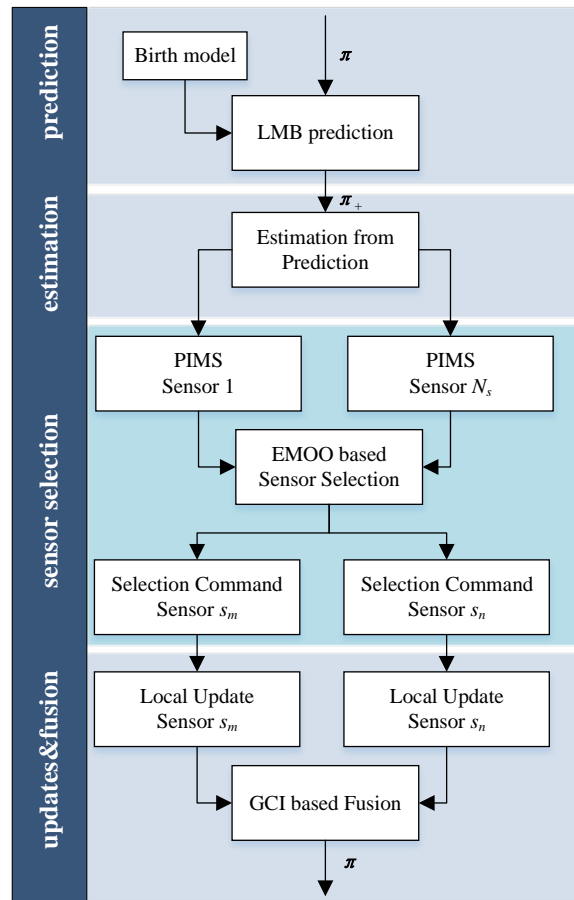


Figure 6. Schematic diagram of sensor selection with LMB filtering.

Algorithm 3 Step-by-step pseudocode for the proposed approach with LMB filtering, sensor selection, and fusion.

INPUTS:

→ LMB distribution $\pi = \{r^{(\ell)}, \{\omega_j^{(\ell)}, x_j^{(\ell)}\}_{j=1}^{J^{(\ell)}}\}_{\ell \in \mathbb{L}}$ from previous time step

OUTPUTS:

→ The posterior parameters $\pi = \{r^{(\ell)}, \{\omega_j^{(\ell)}, x_j^{(\ell)}\}_{j=1}^{J^{(\ell)}}\}_{\ell \in \mathbb{L}}$ to be propagated to the next time step

→ Estimated multi-target states at the current time

1. Predict the LMB distribution $\pi_+ = \{(r_+^{(\ell)}, p_+^{(\ell)}(\cdot))\}_{\ell \in \mathbb{L}_+}$ using (12)–(14)
2. Estimate the target states \hat{X} using $\pi_+ = \{(r_+^{(\ell)}, p_+^{(\ell)}(\cdot))\}_{\ell \in \mathbb{L}_+}$ based on (29) and (30)
3. **for** every sensor $s_i \in N_s$ **do**
4. Compute the PIMS $Z^{(i)}$ of sensor s_i
5. **end for**
6. EMOO-based sensor selection
7. Collect $Z^{(s^*)}$ from the selected sensors s^*
8. **for** every sensor $s_i \in s^*$ **do**
9. Update the local LMB distribution $\pi(\cdot|Z^{(s_i)}) = \{(r_{i,s_i}^{(\ell)}, p_{i,s_i}^{(\ell)}(\cdot))\}_{\ell \in \mathbb{L}_+}$ using (17)–(23)
10. **end for**
11. Obtain the posterior distribution $\hat{\pi}(\cdot|Z^{(s)}) = \{r^{(\ell)}, \{\omega_j^{(\ell)}, x_j^{(\ell)}\}_{j=1}^{J^{(\ell)}}\}_{\ell \in \mathbb{L}}$ based on the GCI method using (37) and (38)
12. Pruning and resampling to obtain the posterior LMB distribution
13. Extract multi-target states using (38) and (39)

Algorithm 4 Step-by-step pseudocode for the EMOO-based sensor selection.

INPUTS:

- The predicted LMB distribution $\pi_+ = \{(r_+^{(\ell)}, p_+^{(\ell)}(\cdot))\}_{\ell \in \mathbb{L}_+}$
- PIMS from each sensor $s_i \in N_s$
- The population size N^{pop}
- The maximum number G of generations

OUTPUTS:

- The sensors s^* selected at current time
1. Initialize population of size N^{pop} , which meet the constraint in (32)
 2. Set the generation $t = 0$
 3. **while** $t < G$
 4. Evaluate individual fitness using (27) and (28)
 5. Create a new population of offspring with the implementation of the tournament selection operator, the proposed binary constrained crossover (Algorithm 1) and binary constrained mutation (Algorithm 2)
 6. Combine the parents and offspring to create the next population
 7. Set $t = t + 1$
 8. **end**
 9. A set of non-dominated solutions is obtained
 10. Select the compromise solution using the GRA strategy (33)–(36)
-

4. Experiments

The performance of the proposed sensor selection approach is demonstrated within a multistatic sensor system. Compared with the traditional monostatic sensor, the multistatic sensor has many advantages [45]; for example, the information on target signatures is enhanced because of the multi-perspective and differences in the clutter properties. What is more, the receive-only multistatic sensor is passive, which provides obvious advantages in military applications. However, measurements collected by the multistatic sensor system are generally affected by noise corruption, missed detections, and false alarms, since its transmit and receive antennas are located in different places.

We use a multistatic sensor system whose structure is borrowed from [46]. As shown in Figure 7a, there is one transmitter and ten receivers within the surveillance system. The receivers are selected adaptively during the tracking of targets. The probability of detection for each receiver $j = 1, 2, \dots, 10$ is modeled as follows [46]

$$p_D^{(j)}(x_k) = 1 - \phi(\|p_k - r^{(j)}\|; \alpha, \beta), \quad (40)$$

where p_k and $r^{(j)}$ denote the target position and the position of receiver j , respectively; $\phi(d; \alpha, \beta) = \int_{-\infty}^d \mathcal{N}(v; \alpha, \beta) dv$ is the Gaussian cumulative distribution function with $\alpha = 12$ km and $\beta = (3 \text{ km})^2$; $\|p_k - r^{(j)}\|$ is the distance between the receiver and the target. Figure 7b plots the contour lines of the detection probability for each sensor in the $x - y$ plane. It can be observed from Figure 7b that the probability of detection for the multistatic sensor system decreases with the increase in the distance [47].

The sampling interval of the system is fixed as $T = 10$ s, and all the receivers have identical measurement noise. The measurement vector consists of a bearing and bistatic range, as follows

$$z_k^j = \begin{bmatrix} \varphi \\ \rho \end{bmatrix} = \begin{bmatrix} \arctan\left(\frac{p_{y,k} - r_y^{(j)}}{p_{x,k} - r_x^{(j)}}\right) \\ \left\|p_k - r^{(j)}\right\| + \left\|p_k - t\right\| \end{bmatrix} + \varepsilon_{k'}^j \quad (41)$$

where $\varepsilon_k^j \sim N(\cdot; 0, R_k)$, with $R_k = \text{diag}([\sigma_\varphi^2, \sigma_\rho^2])$ and $\sigma_\varphi = (\pi/180)$ rad, $r^{(j)} = [r_x^{(j)}, r_y^{(j)}]^T$, and $\sigma_\rho = 5$ m. The clutter measurements are uniformly distributed in $[-\pi, \pi]$ rad \times $[0, 15,000]$ m with $\kappa = 2 \times 10^{-5}(\text{radm})^{-1}$.

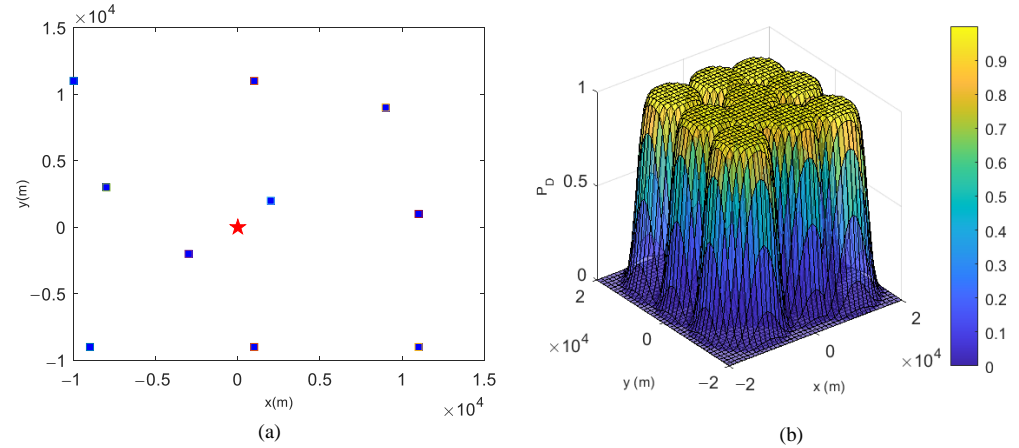


Figure 7. Simulation setup: (a) The locations of the transmitter (star) and receivers (squares); (b) contour plot of the probability of detection.

We use two MTT scenarios to study the performance of the EMOO approach. The first scenario has a time-varying number of targets moving with nearly constant turn (NCT) motion. The second scenario consists of three targets moving with nearly constant velocity (NCV) motion. To evaluate the performance of the EMOO approach, we compare it with three sensor selection solutions: (i) the heuristic random selection method, in which each sensor has an equal probability of being chosen; (ii) the variance-based approach using the cardinality variance defined in (28) as the cost function; (iii) the Cauchy–Schwarz divergence-based approach, which uses the Cauchy–Schwarz divergence between the predicted and updated LMB densities as the reward function. The traditional exhaustive search scheme is used to find the selection command in methods (ii) and (iii), in which the objective function is computed for all possible combinations of a fixed number of sensors in the MSS. In the following, a fixed number $N = 3$ of sensors are selected in these comparative algorithms.

The average tracking performances are obtained using 100 Monte Carlo (MC) runs. The optimal sub-pattern assignment (OSPA) [48] and OSPA⁽²⁾ [49,50] distances are used to evaluate the tracking errors. By measuring the distance between two sets of states, the OSPA metric [48] can estimate errors in both cardinality and localization. As an adaptation of the OSPA metric, the OSPA⁽²⁾ metric [49,50] considers sets of tracks and carries the interpretation of a per-track per-time error. All experiments are tested in Matlab R2010a and implemented on a computer with a 3.40 GHz processor.

4.1. Scenario 1

In this scenario, the tracking of two targets with NCT motion is studied. The target state vector is $x_k := [p_{x,k}, \dot{p}_{x,k}, p_{y,k}, \dot{p}_{y,k}, \omega_k]^T$, in which ω_k is the turn rate. The transition model is

$$x_k = f(x_{k-1}) + Gw_{k-1}, \quad (42)$$

where

$$f(x_{k-1}) = F(\omega_{k-1})x_{k-1}, \quad (43)$$

$$F(\omega_{k-1}) = \begin{bmatrix} 1 & \frac{\sin \omega_{k-1}T}{\omega_{k-1}} & 0 & -\frac{1-\cos \omega_{k-1}T}{\omega_{k-1}} & 0 \\ 0 & \cos \omega_{k-1}T & 0 & -\sin \omega_{k-1}T & 0 \\ 0 & \frac{1-\cos \omega_{k-1}T}{\omega_{k-1}} & 1 & \frac{\sin \omega_{k-1}T}{\omega_{k-1}} & 0 \\ 0 & \sin \omega_{k-1}T & 0 & \cos \omega_{k-1}T & 0 \\ 0 & 0 & 0 & 0 & 1 \end{bmatrix}, \tag{44}$$

$$G = \begin{bmatrix} \frac{T^2}{2} & 0 & 0 \\ T & 0 & 0 \\ 0 & \frac{T^2}{2} & 0 \\ 0 & T & 0 \\ 0 & 0 & T \end{bmatrix}, \tag{45}$$

$$w_{k-1} := [w_{x,k-1}, w_{y,k-1}, w_{\omega,k-1}]^T, \tag{46}$$

and $w_{k-1} \sim \mathcal{N}(w_{k-1}; 0, Q_{k-1})$ is white Gaussian process noise with covariance $Q_{k-1} = \text{diag}(\sigma_x^2, \sigma_y^2, \sigma_\omega^2)$, where $\sigma_x = \sigma_y = 1.0 \times 10^{-4} \text{ m/s}^2$ and $\sigma_\omega = 1.0 \times 10^{-9} \text{ rad/s}^2$. The covariance of the additive process noise Gw_{k-1} is $GQ_{k-1}G^T$.

The birth process follows the LMB distribution $\{(r_B, p_B^{(i)})\}_{i=1}^2$, where $r_B = 0.02$ and $p_B^{(i)} = \mathcal{N}(x; m_B^{(i)}, P_B)$ with the mean $m_B^{(1)} = [2500, 0, -1000, 0, 0]^T$, $m_B^{(2)} = [1750, 0, 1000, 0, 0]^T$, and the covariance $P_B = \text{diag}([50, 50, 50, 50, 6(\pi/180)]^T)^2$. The units are meters for x and y and meters per second for \dot{x} and \dot{y} . The maximum and minimum numbers of particles for each hypothesized track are $L_{\max} = 1000$ and $L_{\min} = 300$, respectively. For each hypothesized track, the number of particles is proportional to its probability of existence. The probability of survival is fixed as $p_S = 0.99$. The number of components for each forward propagation is set to 100. The ground truth and estimated tracks for a single MC run with $N_{\min} = 1$ and $N_{\max} = 3$ is illustrated in Figure 8, showing the true and estimated tracks in x and y coordinates versus time. The plots indicate that the EMOO approach is able to identify target births and successfully accommodate nonlinearities.

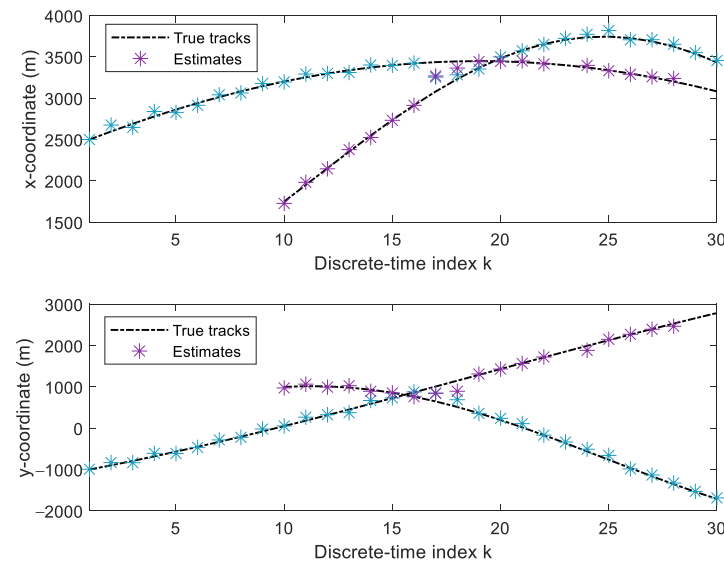


Figure 8. True and estimated tracks versus time in Scenario 1.

The average OSPA error (with parameters $p = 1$ and $c = 300 \text{ m}$) and $\text{OSPA}^{(2)}$ error (with the same c, p , and window length $w = 10$) are given in Figure 9a,b, respectively. The average number of selected sensors is shown in Figure 9c. We observe that both the variance-based approach and the proposed EMOO approach outperform the Cauchy–Schwartz divergence-based approach in terms of OSPA and $\text{OSPA}^{(2)}$ errors. This is mainly because the objective functions of the variance-based approach and the EMOO approach are derived from the cardinality distribution, which is strongly related to the error terms computed in

OSPA and $OSPA^{(2)}$ metrics. In addition, the detection probability is unsatisfactory in the considered scenario. This underlines the importance of cardinality estimation, which is the focus of the objective function developed for the variance-based approach and the EMOO approach. Compared with the variance-based approach, the EMOO approach uses fewer sensors at each time step (as shown in Figure 9c) but provides better tracking accuracy (as shown in Figure 9a,b). For the variance-based approach, a fixed number of $N = 3$ sensors are selected at each time step. However, using more sensors does not indicate a better tracking performance. When the uncertainty of the multi-sensor tracking system is high, such as the scenario we consider, using more sensors for tracking may reduce the tracking performance.

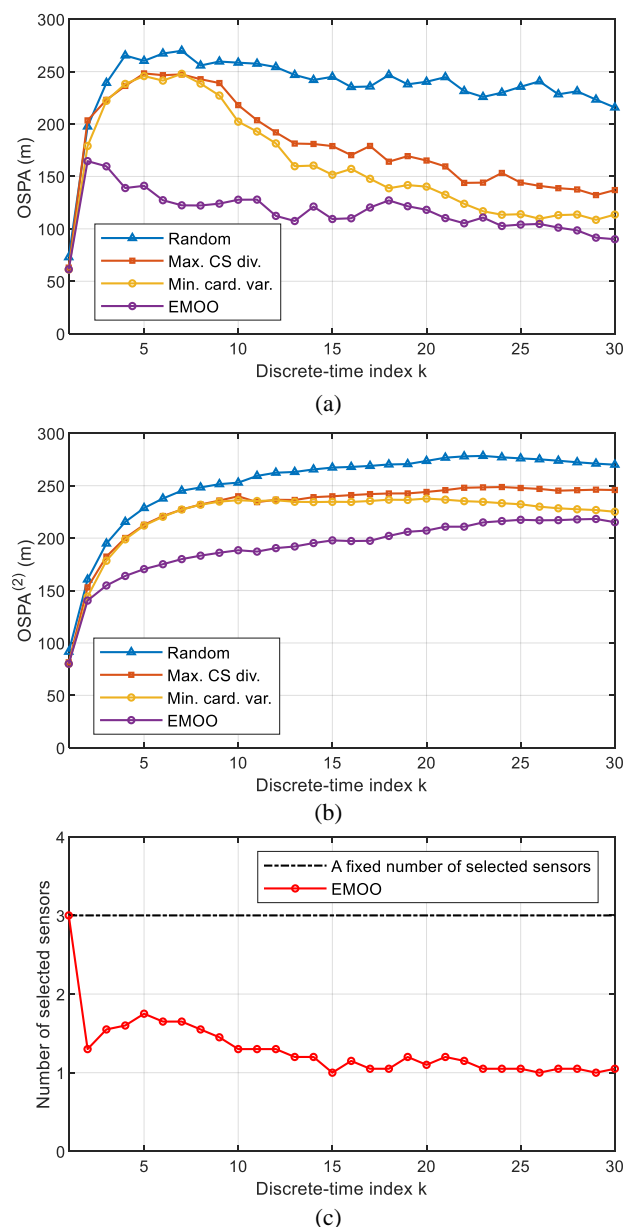


Figure 9. Average performance comparison in Scenario 1: (a) OSPA error; (b) $OSPA^{(2)}$ error; (c) the number of selected sensors.

The average computing times for the random selection approach, the CS divergence-based approach, the cardinality variance-based approach, and the EMOO approach to execute a complete MC simulation are 2.14, 153.28, 194.76, and 87.02 s, respectively. Compared with other methods, the random selection method requires less computing time

because it does not use any technical method. The EMOO approach runs faster than the CS divergence-based approach and the cardinality variance-based approach.

4.2. Scenario 2

In this scenario, three targets with NCV motion move into the surveillance area. The state of the moving target at time k is denoted as $x_k = [p_{x,k}, \dot{p}_{x,k}, p_{y,k}, \dot{p}_{y,k}]^T$. The NCV motion of each target is modeled as

$$x_k = F_{k-1}x_{k-1} + w_{k-1}, \tag{47}$$

where

$$F_{k-1} = \begin{bmatrix} 1 & T & 0 & 0 \\ 0 & 1 & 0 & 0 \\ 0 & 0 & 1 & T \\ 0 & 0 & 0 & 1 \end{bmatrix}, \tag{48}$$

and w_{k-1} is white Gaussian process noise with covariance Q_{k-1} denoted as

$$Q_{k-1} = \sigma_w^2 \begin{bmatrix} \frac{T^4}{4} & \frac{T^3}{2} & 0 & 0 \\ \frac{T^3}{2} & T^2 & 0 & 0 \\ 0 & 0 & \frac{T^4}{4} & \frac{T^3}{2} \\ 0 & 0 & \frac{T^3}{2} & T^2 \end{bmatrix}, \tag{49}$$

and $\sigma_w = 0.01 \text{ m/s}^2$ is the standard deviation of the acceleration noise.

The birth process is an LMB RFS with parameters $\{(r_B, p_B^{(i)})\}_{i=1}^3$, where $r_B = 0.02$ and $p_B^{(i)} = \mathcal{N}(x; m_B^{(i)}, P_B)$ with $m_B^{(1)} = [3000, 0, 0, 0]^T$, $m_B^{(2)} = [2250, 0, 2000, 0]^T$, $m_B^{(3)} = [3000, 0, 2500, 0]^T$, and $P_B = \text{diag}([50, 50, 50, 50]^T)^2$. The units of these elements are the same as those in Scenario 1. The position estimates for a single run of the EMOO approach, assuming $N_{\min} = 1$ and $N_{\max} = 3$, are illustrated in Figure 10. It can be observed that the trajectory estimates of the EMOO approach are close to the true trajectories.

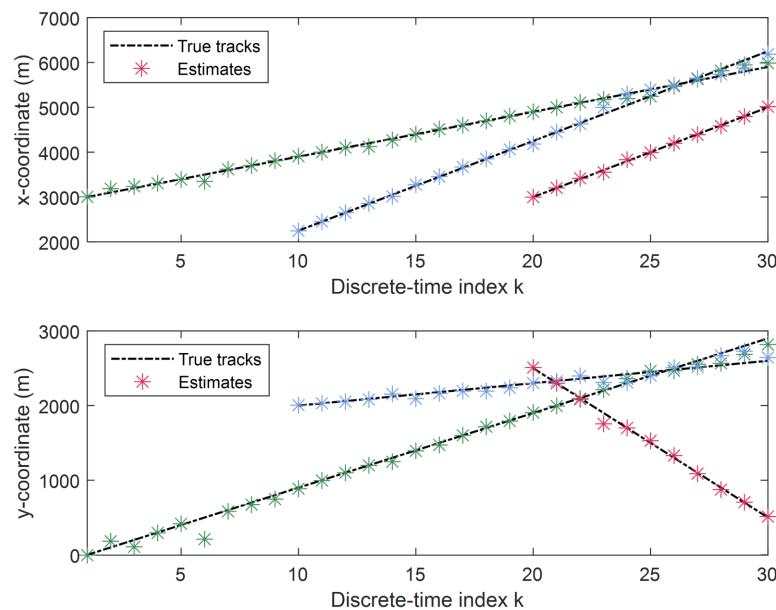


Figure 10. True and estimated tracks versus time in Scenario 2.

The average OSPA and OSPA⁽²⁾ errors (with the same parameters as used in Scenario 1) are given in Figure 11a,b, respectively. The average number of selected sensors is shown in Figure 11c. It can be observed that the tracking errors of the EMOO approach are less

than those of other methods in terms of OSPA and OSPA⁽²⁾. Although the variance-based approach and the proposed EMOO method converge to similar error values, the error of the latter arrives there much earlier. Figure 11c shows that the number of selected sensors for the EMOO method is always less than that of other methods. The average computing times for the random selection approach, the CS divergence-based approach, the cardinality variance-based approach, and the EMOO approach to execute a complete MC simulation are 3.29, 279.85, 343.79, and 157.66 s, respectively. Referring to the tracking accuracy, computing time, and the number of selected sensors, the EMOO approach provides an alternative solution for sensor selection.

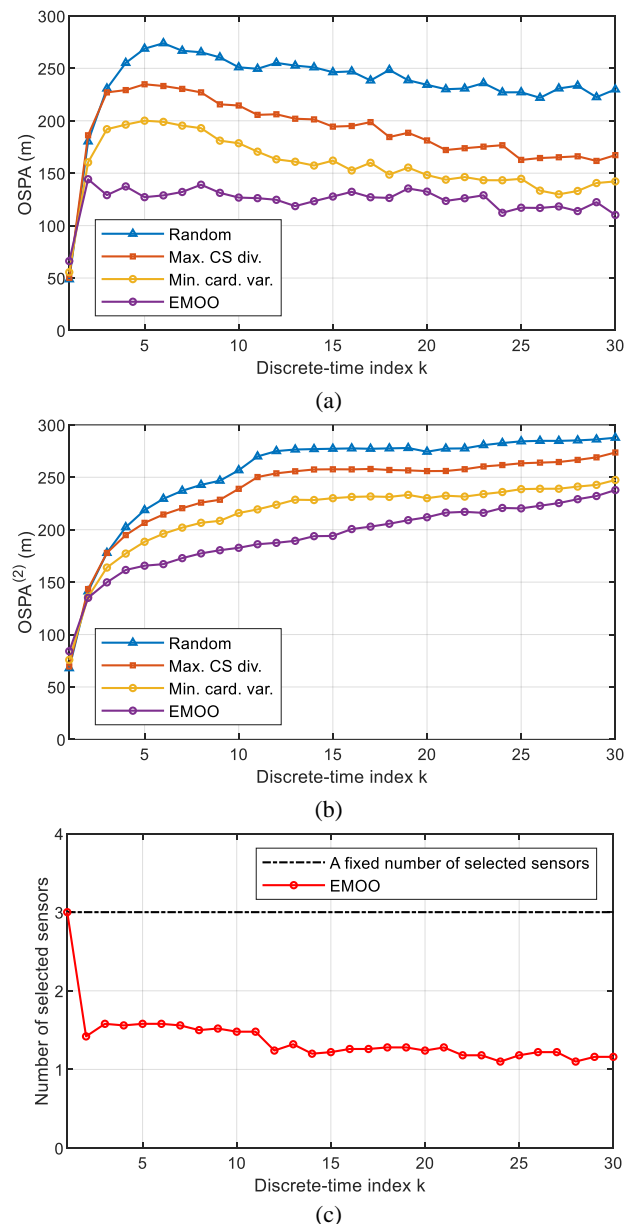


Figure 11. Average performance comparison in Scenario 2: (a) OSPA error; (b) OSPA⁽²⁾ error; (c) the number of selected sensors.

5. Discussion

In the above experiments, we use two different MTT scenarios with the NCV and NCT target motions to demonstrate the performances of the proposed EMOO approach. The OSPA and OSPA⁽²⁾ errors are used to measure the tracking accuracy, which is widely used in the RFS-based tracking field. The average tracking results obtained over 100 MC runs

show that the EMOO approach performs better than the existing methods in terms of the OSPA and OSPA⁽²⁾ errors. What is more, the EMOO approach can significantly reduce the number of selected sensors at each time step. Therefore, the energy and bandwidth problems can be effectively alleviated. The experimental results are well consistent with previous theoretical analysis.

6. Conclusions

A novel sensor selection approach based on evolutionary computational intelligence has been proposed under the FISST framework. The multi-target state is modeled by the LMB RFS, and the posterior density is propagated using the LMB filtering. We model the sensor selection problem as an EMOO problem with two conflicting objective functions, i.e., the number of selected sensors and the cardinality variance. The selection command is determined by optimizing the MOO problem using a novel binary constrained evolutionary algorithm. The performance of the proposed EMOO approach was verified using two scenarios in which a multistatic sensor system with poor detection ability is used for MTT. Simulation results demonstrate that the EMOO approach performs better than existing methods in terms of OSPA and OSPA⁽²⁾ errors and significantly reduces the number of selected sensors. Our future work will consider integrating data from multiple scans to improve the tracking performance. Furthermore, the proposed EMOO methodology also applies to other advanced RFS filters such as GLMB, and this is another direction for future work.

Author Contributions: Conceptualization, S.L. and Y.Z.; methodology, S.L. and Y.Z.; software, Y.Z. and S.L.; validation, Y.Z., S.L., H.L. and J.Y.; formal analysis, H.L.; investigation, Y.Z. and S.L.; resources, Y.Z. and S.L.; data curation, Y.Z. and S.L.; writing—original draft preparation, Y.Z., S.L. and H.L.; writing—review and editing, H.L. and J.Y.; visualization, Y.Z.; supervision, Y.Z. and S.L.; project administration, Y.Z. and S.L.; funding acquisition, Y.Z., S.L. and H.L. All authors have read and agreed to the published version of the manuscript.

Funding: This work was supported in part by the National Natural Science Foundation of China under grant numbers 62007022 and 61906146, the Natural Science Foundation of Shaanxi Province under grant number 2021JQ-209, and the Fundamental Research Funds for the Central Universities under grant number GK202103082 and JB210210.

Data Availability Statement: In this work, we have used the free RFS MATLAB code provided by Prof. Ba-Ngu Vo and Prof. Ba-Tuong Vo at <http://ba-tuong.vo-au.com/codes.html> (accessed on 5 July 2022).

Conflicts of Interest: The authors declare no conflict of interest.

References

1. Gao, J.; Zhang, Q.; Sun, H.; Wang, W. A Multi-Sensor Interacted Vehicle-Tracking Algorithm with Time-Varying Observation Error. *Remote Sens.* **2022**, *14*, 2176. [[CrossRef](#)]
2. Memon, S.A.; Ullah, I.; Khan, U.; Song, T.L. Smoothing Linear Multi-Target Tracking Using Integrated Track Splitting Filter. *Remote Sens.* **2022**, *14*, 1289. [[CrossRef](#)]
3. Mallick, M.; Krishnamurthy, V.; Vo, B.N. *Integrated Tracking, Classification, and Sensor Management: Theory and Applications*; Wiley Press: Hoboken, NJ, USA, 2012.
4. Bar-Shalom, Y.; Willett, P.; Tian, X. *Tracking and Data Fusion: A Handbook of Algorithms*; YBS Publishing: Storrs, CT, USA, 2011.
5. Mahler, R. Global Posterior Densities for Sensor Management. In *Acquisition, Tracking, and Pointing XII*; SPIE: Bellingham, WA, USA, 1998; pp. 252–263.
6. Reid, D. An Algorithm for Tracking Multiple Targets. *IEEE Trans. Autom. Control* **1979**, *24*, 843–854. [[CrossRef](#)]
7. Kurien, T. Issues in The Design of Practical Multitarget Tracking Algorithms. In *Multitarget-Multisensor Tracking: Advanced Applications*; Bar-Shalom, Y., Ed.; Artech House: Norwood, MA, USA, 1990; pp. 43–83.
8. Fortmann, T.; Bar-Shalom, Y.; Scheffe, M. Sonar Tracking of Multiple Targets Using Joint Probabilistic Data Association. *IEEE J. Ocean. Eng.* **2003**, *8*, 173–184. [[CrossRef](#)]
9. Mahler, R. *Statistical Multisource-Multitarget Information Fusion*; Artech House: Norwood, MA, USA, 2007.
10. Mahler, R. *Advances in Statistical Multisource-Multitarget Information Fusion*; Artech House: Norwood, MA, USA, 2014.

11. Mahler, R. Multitarget Bayes Filtering via First-order Multitarget Moments. *IEEE Trans. Aerosp. Electron. Syst.* **2003**, *39*, 1152–1178. [[CrossRef](#)]
12. Mahler, R. PHD Filters of Higher Order in Target Number. *IEEE Trans. Aerosp. Electron. Syst.* **2007**, *43*, 1523–1543. [[CrossRef](#)]
13. Vo, B.T.; Vo, B.N.; Cantoni, A. The Cardinality Balanced Multi-Target Multi-Bernoulli Filter and Its Implementations. *IEEE Trans. Signal Process.* **2009**, *57*, 409–423.
14. Vo, B.T.; Vo, B.N. Labeled Random Finite Sets and Multi-Object Conjugate Priors. *IEEE Trans. Signal Process.* **2013**, *61*, 3460–3475. [[CrossRef](#)]
15. Vo, B.T.; Vo, B.N. A Random Finite Set Conjugate Prior and Application to Multi-target Tracking. In Proceedings of the 2011 7th International Conference on Intelligent Sensors, Sensor Networks and Information Processing, Adelaide, SA, Australia, 6–9 December 2011; pp. 431–436.
16. Vo, B.N.; Vo, B.T.; Phung, D. Labeled Random Finite Sets and the Bayes Multi-Target Tracking Filter. *IEEE Trans. Signal Process.* **2014**, *62*, 6554–6567. [[CrossRef](#)]
17. Reuter, S.; Vo, B.T.; Vo, B.N.; Dietmayer, K. The Labeled Multi-Bernoulli Filter. *IEEE Trans. Signal Process.* **2014**, *62*, 3246–3260.
18. Hero, A.O.; Kreucher, C.M.; Blatt, D. Information Theoretic Approaches to Sensor Management. In *Foundations and Applications of Sensor Management*; Hero, A.O., Castanon, D., Cochran, D., Kastella, K., Eds.; Springer: Berlin/Heidelberg, Germany, 2008; Chapter 3, pp. 33–57.
19. Ristic, B.; Vo, B. Sensor Control for Multi-object State-space Estimation Using Random Finite Sets. *Automatica* **2010**, *46*, 1812–1818. [[CrossRef](#)]
20. Cai, H.; Gehly, S.; Yang, Y.; Hoseinnezhad, R.; Norman, R.; Zhang, K. Multisensor Tasking Using Analytical Renyi Divergence in Labeled Multi-Bernoulli Filtering. *J. Guid. Control Dyn.* **2019**, *42*, 2078–2085. [[CrossRef](#)]
21. Hoang, H.G.; Vo, B.N.; Vo, B.T.; Mahler, R. The Cauchy-Schwarz Divergence for Poisson Point Processes. *IEEE Trans. Inf. Theory* **2015**, *61*, 4475–4485. [[CrossRef](#)]
22. Beard, M.; Vo, B.T.; Vo, B.N.; Arulampalam, S. Void Probabilities and Cauchy-Schwarz Divergence for Generalized Labeled Multi-Bernoulli Models. *IEEE Trans. Signal Process.* **2017**, *65*, 5047–5061. [[CrossRef](#)]
23. Gostar, A.K.; Hoseinnezhad, R.; Bab-Hadiashar, A.; Liu, W. Sensor-Management for Multitarget Filters via Minimization of Posterior Dispersion. *IEEE Trans. Aerosp. Electron. Syst.* **2017**, *53*, 2877–2884. [[CrossRef](#)]
24. Nguyen, H.V.; Rezatofighi, H.; Vo, B.N.; Ranasinghe, D.C. Online UAV Path Planning for Joint Detection and Tracking of Multiple Radio-Tagged Objects. *IEEE Trans. Signal Process.* **2019**, *67*, 5365–5379. [[CrossRef](#)]
25. Jiang, M.; Yi, W.; Kong, L. Multi-sensor Control for Multi-target Tracking Using Cauchy-Schwarz Divergence. In Proceedings of the 2016 19th International Conference on Information Fusion (FUSION), Heidelberg, Germany, 5–8 July 2016; pp. 2059–2066.
26. Hoang, H.G.; Vo, B.T. Sensor Management for Multi-target Tracking via Multi-Bernoulli Filtering. *Automatica* **2014**, *50*, 1135–1142. [[CrossRef](#)]
27. Gostar, A.K.; Hoseinnezhad, R.; Bab-Hadiashar, A. Multi-Bernoulli Sensor Control via Minimization of Expected Estimation Errors. *IEEE Trans. Aerosp. Electron. Syst.* **2015**, *51*, 1762–1773. [[CrossRef](#)]
28. Panicker, S.; Gostar, A.K.; Bab-Hadiashar, A.; Hoseinnezhad, R. Sensor Control for Selective Object Tracking Using Labeled Multi-Bernoulli Filter. In Proceedings of the 2018 21st International Conference on Information Fusion (FUSION), Cambridge, UK, 10–13 July 2018; pp. 2218–2224.
29. Panicker, S.; Gostar, A.K.; Bab-Hadiashar, A.; Hoseinnezhad, R. Tracking of Targets of Interest Using Labeled Multi-Bernoulli Filter with Multi-Sensor Control. *Signal Process.* **2020**, *171*, 107451. [[CrossRef](#)]
30. Nguyen, H.V.; Rezatofighi, H.; Vo, B.N.; Ranasinghe, D. Multi-Objective Multi-Agent Planning for Jointly Discovering and Tracking Mobile Object. In Proceedings of the AAAI Conference on Artificial Intelligence, New York, NY, USA, 7–12 February 2020; pp. 7227–7235.
31. Zhu, Y.; Wang, J.; Liang, S. Multi-Objective Optimization Based Multi-Bernoulli Sensor Selection for Multi-Target Tracking. *Sensors* **2019**, *19*, 980. [[CrossRef](#)]
32. Ma, L.; Xue, K.; Wang, P. Multitarget Tracking with Spatial Nonmaximum Suppressed Sensor Selection. *Math. Probl. Eng.* **2015**, *2015*, 148081. [[CrossRef](#)]
33. Ma, L.; Xue, K.; Wang, P. Distributed Multiagent Control Approach for Multitarget Tracking. *Math. Probl. Eng.* **2015**, *2015*, 903682. [[CrossRef](#)]
34. Wang, X.; Hoseinnezhad, R.; Gostar, A.K.; Rathnayake, T.; Xu, B.; Bab-Hadiashar, A. Multi-sensor Control for Multi-object Bayes Filters. *Signal Process.* **2018**, *142*, 260–270. [[CrossRef](#)]
35. Cao, N.; Choi, S.; Masazade, E.; Varshney, P.K. Sensor Selection for Target Tracking in Wireless Sensor Networks with Uncertainty. *IEEE Trans. Signal Process.* **2016**, *64*, 5191–5204. [[CrossRef](#)]
36. Fantacci, C.; Vo, B.N.; Vo, B.T.; Battistelli, G.; Chisci, L. Consensus Labeled Random Finite Set Filtering for Distributed Multi-Object Tracking. *arXiv* **2015**, arXiv:1501.01579.
37. Mahler, R. Multitarget Sensor Management of Dispersed Mobile Sensors. In *Theory and Algorithms for Cooperative Systems*; Grundle, D., Murphey, R., Pardalos, P.M., Eds.; World Scientific: Singapore, 2004; pp. 239–310.
38. Li, H.; Gong, M.; Wang, C.; Miao, Q. Pareto Self-Paced Learning Based on Differential Evolution. *IEEE Trans. Cybern.* **2021**, *51*, 4187–4200. [[CrossRef](#)]

39. Gong, M.; Li, H.; Luo, E.; Liu, J.; Liu, J. A Multiobjective Cooperative Coevolutionary Algorithm for Hyperspectral Sparse Unmixing. *IEEE Trans. Evol. Comput.* **2017**, *21*, 234–248. [[CrossRef](#)]
40. Gong, M.; Li, H.; Meng, D.; Miao, Q.; Liu, J. Decomposition-Based Evolutionary Multiobjective Optimization to Self-Paced Learning. *IEEE Trans. Evol. Comput.* **2019**, *23*, 288–302. [[CrossRef](#)]
41. Ma, L.; Gong, M.; Yan, J.; Yuan, F. A Decomposition-based Multiobjective Evolutionary Algorithm for Analyzing Network Structural Balance. *Inf. Sci.* **2017**, *378*, 144–160. [[CrossRef](#)]
42. Ngatchou, P.; Zarei, A.; El-Sharkawi, A. Pareto Multi-Objective Optimization. In Proceedings of the 2005 13th International Conference on Intelligent Systems Application to Power Systems, Arlington, VA, USA, 6–10 November 2005; pp. 84–91.
43. Deng, J.L. Control Problems of Grey Systems. *Syst. Control Lett.* **1982**, *1*, 288–294.
44. Ristic, B.; Arulampalam, S.; Gordon, N. *Beyond the Kalman Filter-Particle Filters for Tracking Applications*; Artech House: Norwood, MA, USA, 2004.
45. Willis, N.J.; Griffiths, H.D. *Advances in Bistatic Radar*; SciTech Publishing Inc.: Raleigh, NC, USA, 2007.
46. Ristic, B.; Farina, A. Target Tracking via Multi-static Doppler Shifts. *IET Radar Sonar Navig.* **2013**, *7*, 508–516.
47. Mahafza, B. *Radar Systems Analysis and Design Using MATLAB*, 3rd ed.; Chapman and Hall/CRC Press: Boca Raton, FL, USA, 2013.
48. Schuhmacher, D.; Vo, B.T.; Vo, B.N. A Consistent Metric for Performance Evaluation of Multi-Object Filters. *IEEE Trans. Signal Process.* **2008**, *56*, 3447–3457. [[CrossRef](#)]
49. Beard, M.; Vo, B.T.; Vo, B.N. A Solution for Large-Scale Multi-Object Tracking. *IEEE Trans. Signal Process.* **2020**, *68*, 2754–2769. [[CrossRef](#)]
50. Beard, M.; Vo, B.T.; Vo, B.N. Performance Evaluation for Large-Scale Multi-Target Tracking Algorithms. In Proceedings of the 2018 21st International Conference on Information Fusion (FUSION), Cambridge, UK, 10–13 July 2018; pp. 1–5.